https://doi.org/10.1016/j.nanoen.2017.04.044

A paper-based electrode using a graphene dot/PEDOT:PSS composite for flexible solar cells

Chuan-Pei Lee[a,b], Kun-Yu Lai[c], Chin-An Lin[a], Chun-Ting Li[d], Kuo-Chuan Ho[d], Chih-I Wu[b],

Shu-Ping Lau[e], Jr-Hau He[a,*]

a Computer, Electrical and Mathematical Sciences and Engineering (CEMSE) Division, King Abdullah, University of Science and Technology (KAUST),

Thuwal 23955-6900, Saudi Arabia

b Institute of Photonics and Optoelectronics and Department of Electrical Engineering, National Taiwan University, Taipei 10617, Taiwan, ROC

c Department of Optics and Photonics, National Central University, Chung-Li 32001, Taiwan, ROC

d Department of Chemical Engineering, National Taiwan University, Taipei 10617, Taiwan, ROC

e Department of Applied Physics, The Hong Kong Polytechnic University, Hong Kong, China

Abstract

We have synthesized a metal-free composite ink that contains graphene dots (GDs) and poly(3,4-ethylenedioxythiophene): polystyrene sulfonate (PEDOT:PSS) that can be used on paper to serve as the counter electrode in a flexible dye-sensitized solar cell (DSSC). This paper-based GD/PEDOT:PSS electrode is low-cost, light-weight, flexible, environmentally friendly, and easy to cut and process for device fabrication. We determined the GD/PEDOT:PSS composite effectively fills the dense micro-pores in the paper substrate, which leads to improved carrier transport in the electrode and a 3-fold enhanced cell efficiency as compared to the paper electrode made with sputtered Pt. Moreover, the DSSC with the paper electrode featuring the GD/PEDOT:PSS composite did not fail in photovoltaic tests even after bending the electrode 150 times, whereas the device made with the Ptbased paper electrode decreased in efficiency by 45% after such manipulation. These exceptional properties make the metal-free GD/PEDOT:PSS composite ink a promising electrode material for a wide variety of flexible electronic applications.

I. Introduction

Flexible electronics have promising applications in wearable tech-nologies that are increasing in popularity and use [1,2]. In terms of ideal flexible substrates, conventional printer paper, which is composed of multiple layers of cellulose fibers, is among the most attractive due to its environmental-friendliness, low-cost, light-weight, and accessibility in terms of roll-to-roll processing [1,3]. These favorable properties have led researchers to develop paper substrates for various applica-tions, including transistors [4], displays [5], sensors [6], memories [7], batteries [8,9], supercapacitors [10–12], and organic solar cells [13,14]. To make paper-based electrochemical devices, it is necessary to develop low-resistance yet electrochemically active paper electrodes via moderate fabrication processes (e.g., a non-sintering process). However, such a method remains elusive considering the insulating, porous, and delicate nature of the fibrous substrate.

For this reason, printed paper is rarely used as an electrode substrate for third-generation solar cells, such as the widely pursued dye-sensitized solar cell (DSSC) [15,16]. DSSCs are a renewable power source with strong potential owing to the fact that they do not rely on expensive or energy-intensive processing methods [17] and can be printed on flexible substrates using roll-to-roll techniques [18–20]. Flexible DSSCs are easy to fabricate, transport, and install [15,21], making them highly competitive in the photovoltaic market despite their lower efficiencies compared to inorganic-based solar devices [15,21]. However, high-performance DSSCs often necessitate a noble metal as the catalyst for the counter electrode [22], such as Pt, which is extremely expensive and thus negates one of the primary attractive features of the DSSC. To expedite the transition of this unique type of solar cell from the laboratory to commercial markets, it may be necessary to develop metal-free electrocatalytic materials for the electrode [23]. Accordingly, there have been several metal-

free electro-catalysts reported in the literature, such as carbon materials [24,25] and conducting polymers [26,27].

It is well know that conducting polymers possess electrical con-ductivity ranging from semiconductors (10−8 Scm-1) to metals (105 Scm-1) [28]. The conjugated structure of conducting polymers contributes to their electrical conductivity through the continuous overlap of π-orbitals along the polymer backbone, enabling the π-electrons to become delocalized with high mobility [29–31]. Thus, conducting polymers have already been reported as potential materials for applications in many electronic devices, such as thin film transistors [32,33], sensors [34,35], molecular electronics, supercapacitors [36–38], electrochromic devices [31,39], etc. Among the conducting poly-mers, poly-3,4-ethylenedioxythiophene (PEDOT) is of particular inter-est due to its high conductivity, electrochemical stability, mechanical flexibility, transparency, catalytic ability, and stability in the oxidized state [40,41]. It has also exhibited strong electrocatalytic behavior toward the redox reaction of the I-/I3- electrolyte, as demonstrated via cyclic voltammetry analysis [42–44]. As a result, researchers have widely incorporated PEDOT as the counter electrode in DSSCs in addition to using it as a hole transport layer in solid-state photovoltaic devices due to its high work function [45,46].

However, PEDOT is not soluble in most solvents, which makes solution processing problematic. To improve the material's processa-bility for industrial production, researchers have incorporated poly(-styrenesulfonate) (PSS) as a counter anion to dope PEDOT. The resulting PEDOT:PSS product can be readily dispersed in water, which makes it possible to form conductive layers on various substrates via solution coating methods [41,47]. Despite this advantage, the materi-al's significantly decreased conductivity and electrocatalytic activity toward I3– reduction due to the addition of the nonconductive PSS counter anion and

the use of flat film surfaces (i.e., low-catalytic area) greatly sacrifices the performance of DSSCs made from PEDOT:PSS counter electrodes [41].

To address this issue, researchers have studied several carbon materials, including carbon black, carbon nanotubes, and graphene to the PEDOT:PSS catalytic film [48–51]. Recently, nano-sized graphene fragments, i.e., graphene dots (GDs), were shown to exhibit exceptional properties of quantum confinement and edge effects, [52] and have been applied to solar-water-splitting [53], bio-imaging [54,55], light emitting diodes [56,57], photovoltaics [58–61], and more. GDs can also be well dispersed in common solvents for various solution-based processes due to the nanoscale-size of this two-dimensional material and the presence of C–OH, C=O, C–O–C, and C–H surface functional groups [57]. The combination of GDs and PEDOT:PSS could therefore enable the fabrication of a more efficient electrocatalytic film at low temperatures (< 100 oC) using a convenient and low-cost solution-coating method.

In this study, we present a DSSC made using a Pt-free counter electrode that features this GD/PEDOT:PSS composite ink. The Pt-free DSSC made with a conducting glass substrate exhibited a cell efficiency of 7.36%, which is the highest ever reported for a DSSC fabricated with a PEDOT:PSS-based counter electrode (see Table S1). Moreover, for the first time, we also demonstrated that this metal-free counter electrode could be fabricated on paper to form a flexible DSSC that exhibits superior performance in terms of efficiency and bending stability compared to the same device made with a Pt-based paper electrode. This novel paper electrode opens a promising pathway for developing next-generation electrochemical and electronic devices that are both flexible and inexpensive.

II. Experiment

Lithium iodide (LiI, synthetic grade) and iodine (I2, synthetic grade) were obtained from Merck. Acetone (99+%), tert-butyl alcohol (tBA, 96%), guanidine thiocyanate (GuSCN, 99+%), and 4-tert-butyl-pyridine (TBP, 96%) were supplied by Acros. Ti(IV)

tetraisopropoxide (TTIP, > 98%), lithium perchlorate (LiClO4, ⩾98.0%), ethanol (> 99.8%), and 2-methoxyethanol (99.95%) were purchased from Sigma-Aldrich. Acetonitrile (ACN, 99.99%) was procured from J. T. Baker. 3-Methoxypropionitrile (MPN, 99%) was purchased from Fluka. 1,2-dimethyl-3-propylimidazolium iodide (DMPII) and cis-diisothio-cyanato-bis (2,2′-bipyridyl-4,4′-dicarboxylato) ruthenium(II) bis(tetra-butylammonium) (N719 dye) were purchased from Solaronix (S.A., Aubonne, Switzerland). An aqueous solution of PEDOT:PSS (PH 500, 1.0–1.4 wt% dispersion in water) was obtained from Heraeus.

We prepared the GDs solution using glucose and deionized water as the carbon source and solvent, respectively [57]. First, we added 2.5 ml of a glucose aqueous solution (8.9 wt%) to a sealed glass bottle, then heated it in a microwave oven at a power of 595 W for 9 min. The glass bottle was then cooled to room temperature.

To optimize the GD/PEDOT:PSS composition, we began with fluorine-doped SnO2 (FTO, TEC-7, 10 Ω sq–1, NSG America Inc., New Jersey, USA) conducting glass as the device substrate. To fabricate the standard counter electrode, we first cleaned the FTO and then sputter coated it with a 5 nm thick Pt layer (~15 s deposition time). To produce a PEDOT:PSS film, we first mixed a solution consisting of 50 vol% of the aqueous PEDOT:PSS dispersion with 50 vol% ethanol. PEDOT:PSS films with various thicknesses (see Fig. S1 in the Supplementary material) were then fabricated on the FTO substrates to form the DSSC counter electrodes via a drop-coating method with a micropipette and subsequent heating at 60 °C for a few hours. The corresponding photovoltaic performances of these devices are shown in Fig. S2. From this study, we determined that a PEDOT:PSS thickness of ~5.25 μm resulted in the best performance, and therefore we adopted that film thickness for all subsequent studies with various GDs contents.

To produce the GD/PEDOT:PSS composite films, we mixed various solutions containing 50 vol% of the aqueous PEDOT:PSS dispersion and 50 vol% of the GDs solution (X) and ethanol (Y) (X=10%, 20%, 30%, and 40%; X+Y=50%). These materials were used to fabricate the corresponding films on the cleaned FTO substrates via drop-coating with subsequent heating at 60 °C for 30 min. After testing a series GDs volume ratios (X) ranging from 10 to 40 vol%, we found that the optimum GDs content in the PEDOT:PSS/ethanol solution was 30 vol%(Fig. S3).

To prepare the paper-based counter electrodes, we used commer-cially available A4 printing paper (Double A) as the substrate. The paper was immersed in the optimal 30 vol% GD/PEDOT:PSS solution for 10 min and then dried at 60 °C for a few hours. This GD/PEDOT:PSS paper composite then served as the counter electrode for the flexible DSSC. For comparison, we also prepared a DSSC using a paper-based electrode made with sputtered Pt as a control. A longer deposition time (~360 s) was used to sputter the Pt due to the extremely rough and porous quality of the paper surface.

For the glass-based DSSC, the conducting surface of the FTO substrate was treated with a solution of TTIP in 2-methoxyethanol (1:3 weight ratio) in order to obtain good contact between the conducting glass and the TiO2 film. To fabricate the mesoporous double-layered TiO2 film on the pre-treated FTO surface, we deposited a transparent 12 μm thick layer of TiO2 particles (20–50 nm diameter, Eversolar P-300) and a 5 μm thick layer of light-scattering TiO2 particles (PST-400, JGC Catalysts and Chemicals, Japan) using a conventional screen-printing method [62]. We formed a 0.4×0.4 cm2 region of the double-layer TiO2 film on the substrate by scrapping away excess material from the sides of this active area. The TiO2 film was gradually heated to 500 °C (10 °C min-1) in ambient atmosphere and then held at this temperature for 30 min. After sintering, the TiO2 electrode was cooled to 80 °C and then immersed in a 5×10-4 M N719 dye solution in a mixed solvent

of ACN/tBA (1:1 volume ratio) at room temperature for 24 h. We then coupled this TiO2 electrode with the counter electrode, separating them using a 25 μm thick Surlyn® film (SX1170-25, Solaronix S.A., Aubonne, Switzerland) and heated the device on a hot plate at 150 °C to seal it. For the electrolyte, we used a mixture of 1.2 M DMPII, 0.35 M I2, 0.1 M GuSCN, and 0.5 M TBP in ACN/MPN (4:1 volume ratio), which was injected into the gap between the two electrodes.

To fabricate the paper-based DSSCs, we deposited the dye-sensi-tized TiO2 film on a conducting plastic substrate made of indium tin oxide and polyethylene naphthalate (ITO-PEN, 13 Ω sq–1, Peccell Technologies) using methods described in previous reports [63–65]. Briefly, we first made a binder-free TiO2 paste by thoroughly dispersing 1 g of commercial titanium dioxide nanoparticles (P25, Degussa) in a 6 ml solution of tBA and deionized water (2:1 volume ratio) by continuously stirring the mixture for 5 days. Then the surface of the ITO-PEN substrate was treated with a solution of TTIP (0.028 g) in ethanol (10 ml) to improve the adhesion between the substrate and the TiO2 film. We then took the binder-free TiO2 paste and coated a 10 μm thick film over a 0.4×0.4 cm2 area on the treated ITO-PEN substrate using the doctor blade technique. These TiO2 films were then gradually heated to a temperature of 120 °C (10 °C min-1) in ambient atmo-sphere and subsequently annealed at 120 oC for 1 h. After annealing and cooling the sample to 80 °C, we then immersed the TiO2/ITO-PEN electrode in a 5×10-4 M N719 dye solution at 55 °C for 1 h. The dye/TiO2/ITO-PEN electrode was then coupled with the GD/PEDOT:PSS/paper counter electrode, separated by a 25 μm thick Surlyn® film.

We investigated the GDs using transmission electron microscopy (TEM, JEM-2100F, JEOL) at an operation voltage of 200 kV. We also used atomic force microscopy (AFM, NanoScope IV, Digital Instruments) under tapping mode, and Fourier transform infrared spectroscopy (FTIR, Perkin-Elmer) using flat pieces of potassium bromide in a spectral range from 500

cm–1 to 4000 cm–1. The composition of the GDs were also verified by X-ray photoelectron spectroscopy (XPS) using a micro-focused (100 μm, 25 W) Al X-ray beam. The Ar+ ion source for XPS (FIG-5CE) was controlled using a floating voltage of 0.2 kV. We characterized the domain structure of the GDs by Raman spectroscopy with 532 nm laser excitation and a P2 system model spectrometer (Lambda Solution, Inc.). The surface morphologies of various catalytic films were determined by field emission scanning electron microscopy (FE-SEM, Nova Nano-SEM 230, FEI, Oregon, USA). The elemental distribution of C and O in the GDs film was analyzed by energy dispersive X-ray spectroscopy (EDS). We also identified the crystallinity of the PEDOT:PSS films using X-ray diffraction (XRD, Rigaku).

For photovoltaic characterization, we masked the surface of the DSSC except for a 0.16 cm2 area and illuminated this region with a class-A quality solar simulator (XES-301S, AM 1.5G, SAN-EI ELECTRIC CO., LTD.). The incident light intensity (100 mW cm-2) was calibrated with a standard Si solar cell (PECSI01, Peccell Technologies, Inc., Yokohama, Japan). We recorded the photoelec-trochemical characteristics of the DSSC using a potentiostat/galvano-stat (PGSTAT 30, Autolab, Eco–Chemie, Netherlands). The incident photo-to-electron conversion efficiency (IPCE) curves were obtained at the short-circuit condition. The light source was a class A quality solar simulator (PEC-L11, AM1.5G, Peccell Technologies, Inc.) and it was focused through a monochromator (Oriel Instrument, model 74100) onto the photovoltaic cell. The monochromator was incremented through the visible spectrum to generate the IPCE (λ)asdefined in Eq. (1),

IPCE( ) = 1240(λJSC /)λ

in which λ is the wavelength, JSC is the short-circuit photocurrent density (mA cm-2) recorded with the potentiostat/galvanostat, and φ is the incident radiative flux (W m-2)

measured with an optical detector (Oriel Instrument, model 71580) and power meter (Oriel Instrument, model 70310).

Cyclic voltammetry (CV) and Tafel polarization curves were mea-sured to investigate the electrocatalytic abilities of the counter electro-des. We carried out CV using a three-electrode system, with the PEDOT:PSS or GD/PEDOT:PSS or sputtered Pt catalytic films serving as the working electrodes, a Pt foil as the counter electrode, and an Ag/Ag+ electrode as the reference electrode in an ACN solution that contained 10 mM I–, 1 mM I2, and 0.1 M LiClO4. The Tafel polarization curves were obtained by symmetrical cells consisting of two identical electrodes (i.e., PEDOT:PSS, GD/PEDOT:PSS, or the sputtered Pt electrode), a 25 μm thick Surlyn® film, and the electrolyte.

3. Results and Discussion

We synthesized the water-soluble GDs (Fig. S4) from an aqueous glucose solution by a microwave-assisted hydrothermal technique that can rapidly produce uniformly-sized GDs [57]. Fig. 1a presents a typical TEM image of the GDs, which display a uniform 3 nm diameter across the sample. A high-resolution TEM image (inset of Fig. 1a) reveals the GDs are highly crystalline. The interlayer spacing is 0.213 nm, which corresponds to the d-spacing of the graphene {1100} planes [53,66]. A histogram of the size distribution of the GDs in Fig. 1a demonstrates the GDs sizes are quite uniform (Fig. 1b). Fig. 1c shows the height profile of the monodisperse GDs as measured by AFM. The average height of three GDs measured (labeled as A, B, and C) was ~2.20 nm, indicating ~10 layers of graphene in each GDs. We analyzed the elemental distribution of C and O in the GDs by EDS and found that the atomic ratio of C/O was 95.32/4.68 (Fig. S5), thus confirming that C is the dominant element in the GDs. Fig. 1d presents the FTIR spectrum of the GDs, in which we observed the presence of O–H (3392 cm-1), C–O (1027 cm-1 and 1076 cm-1), C=C (1641 cm-1), and C–H (1360 cm-1

and 2927 cm-1) bonds in the sample [57].We further confirmed the composition of the GDs by XPS (Fig. 1e). The XPS spectrum was deconvoluted into five surface components, including sp2 carbon (C=C) at a binding energy of 284.3 eV, sp3 (C–C and C–H at 285.8 eV, C–OH at 286.2 eV, C–O–C at 287.4 eV, and finally C=O at 288.6 eV. These findings of the GDs surface chemistry are consistent with the FTIR results. Fig. 1f shows the Raman spectrum of the GDs, which exhibited a prominent G band at 1573 cm-1. This peak is due to the first-order scattering of the E2g mode in sp2 carbon domains. The broad D band at 1364 cm-1 is caused by the sp3 hybridized carbon (such as edge planes and structural defects), which breaks the selection rule and reduces the peak symmetry [62,67]. The high intensity ratio of the D band to the G band (ID/IG=0.93) in the Raman spectrum suggests the GDs feature high defect densities [68], which can be beneficial for their electrocatalytic activity [62,69].

Fig. 2a–c present SEM images of the counter electrodes that have been made with Pt, PEDOT:PSS, and 30 vol% GD/PEDOT:PSS films on the FTO substrates. In Fig. 2a, we can see clear domain boundaries of the FTO layer and sputtered Pt nanoparticles uniformly distributed across the surface. In contrast, the PEDOT:PSS film featured a smooth surface, which can be unfavorable for electrocatalytic reactions (Fig. 2b). However, the 30 vol% GD/PEDOT:PSS film exhibited an irregular island-like surface texture (Fig. 2c). Fig. 2d shows the XRD patterns of PEDOT:PSS and 30 vol% GD/PEDOT:PSS films. PEDOT:PSS films made from commercial PEDOT:PSS solutions are typically amorphous [41], unless the film is synthesized via electro-chemical polymerization [70] or annealed at a temperature greater than 100 °C [41,70], in which case sharp diffraction peaks can be observed in the material's XRD pattern. In our work, both PEDOT:PSS and 30 vol% GD/PEDOT:PSS films were prepared via a simple “soak and dry” process, and therefore we observe relatively broad diffraction peaks. After the incorporation of GDs in the PEDOT:PSS film, the XRD 2θ scan showed enhanced diffraction intensities at 19.01° and 26.25°, which are the same as the

PEDOT diffraction pattern reported in an earlier study [40], indicating the improved crystallinity of the compo-site film as compared to that of the pristine PEDOT:PSS. This result suggests that GDs could act as nucleation sites during the film formation process [60]. The presence of nucleation sites in a con-ductive polymer film can lead to the formation of a “nano-island” surface texture, thus resulting in a roughed surface morphology [60].It has been reported that catalytic films featuring high surface roughness on the counter electrode help to promote the electrocatalytic reduction of I3– in DSSCs [60,71]. Meanwhile, we observed that the PEDOT:PSS film exhibited reduced sheet resistance after the incorporation of 30 vol% GDs (from RS=9.6×10-4 Ω cm to RS=1.5×10-4 Ω cm). Accordingly, we expected the DSSC made with the 30 vol% GD/PEDOT:PSS film to have better electrocatalytic performance as compared to that of the cell made with just PEDOT:PSS.

We next measured the photocurrent density-voltage (J-V) charac-teristics of the DSSCs made using the three different counter electrodes (i.e., sputtered Pt, PEDOT:PSS, and 30 vol% GD/PEDOT:PSS) on the FTO substrates, as shown in Fig. 2e. The corresponding photovoltaic parameters are listed in Table 1. The results show that the cell efficiency (η) of the DSSC made with the 30 vol% GD/PEDOT:PSS film (7.36%) was much higher than that of the cell made using just PEDOT:PSS as the counter electrode (5.14%), and was comparable to that of the cell with the sputtered Pt counter electrode (8.46%). Therefore, the performance of the PEDOT:PSS-based counter electrode can be significantly enhanced after the incorporation of the GDs (43%enhancement in cell efficiency).

The differences in η among the three devices were mainly due to their short-circuit photocurrent densities (JSC) and fill factors (FF)(Table 1). Since the photoanode and electrolyte conditions were identical for all the devices, the value of JSC should therefore

depend strictly on the electrocatalytic activity of the counter electrodes. The quick electrocatalytic reduction of the I3– ions leads to fast electron transfer kinetics in the cell and thus also increases FF. In the inset of Fig. 2e, we also measured the IPCE curves of the three devices and found that they exhibited a broad peak across the visible region (400–800 nm), which is typical for DSSCs. The trend in the IPCE plots was also consistent with the corresponding JSC values.

To verify the mechanism of electrocatalytic activity, we analyzed the three electrode types using CV and Tafel plots. Fig. 2f shows the CV curves of the electrodes made with the sputtered Pt, PEDOT:PSS, and 30 vol% GD/PEDOT:PSS films. The corresponding cathodic current density and peak separation (ΔEP) values are listed in Table 2. The cathodic current densities of the sputtered Pt (−1.85 mA cm–2) and 30 vol% GD/PEDOT:PSS (−1.58 mA cm–2) samples were much larger than that of the bare PEDOT:PSS (−0.39 mA cm–2) film. Typically, electrodes with enlarged active surface area and conductivity increase the reduction reaction of I3-, which enhances the cathodic current density and therefore boosts JSC and η for the pertinent DSSCs. As for ΔEP, the values of the sputtered Pt (324 mV) and 30 vol% GD/PEDOT:PSS (347 mV) samples were smaller than that of PEDOT:PSS (436 mV). Since the peak separation of the I–/I3– redox reaction is inversely related to the charge transfer rate of the electrode [22], the results of the ΔEP measurements indicate that the charge transfer rate in the PEDOT:PSS film was the slowest among the three samples, causing it to have the lowest FF value in Table 1.

Fig. 2g shows the Tafel polarization curves obtained using symme-trical cells consisting of two identical electrodes of the three catalytic films. In the Tafel plot, the exchange current density (j0) can be obtained by extrapolating the anodic and cathodic curves to the cross point at 0 V. j0 can be used to calculate the charge transfer resistance (RCt) corresponding to the catalytic film/electrolyte interface according to Eq. (2):

in which n is the electron transfer number for the reduction of I3–, F is the Faraday constant, R is the ideal gas constant, and T is the absolute temperature. A smaller RCt value refers to better charge transfer at the catalytic film/electrolyte interface, or in other words, superior electro-catalytic ability. As listed in Table 2, the electrodes made using 30 vol%GD/PEDOT:PSS had a 29% smaller RCt value compared to that of the PEDOT:PSS sample, which indicates that the addition of GDs to the film improves the electrocatalytic capability of the electrode. This result is consistent with the CV measurements and the corresponding photovoltaic performances listed in Table 1.

To further explore the advantages of the GD/PEDOT:PSS compo-site ink, we also fabricated flexible DSSCs using paper-based counter electrodes made with either 30 vol% GD/PEDOT:PSS (Fig. 3a) or sputtered Pt (Fig. 3b), both of which utilized the flexible dye/TiO2/ITO-PEN photoanode (Fig. 3c). Fig. 3a(i)–(iv) present images of the flexible paper-based electrode made with the 30 vol% GD/PEDOT:PSS ink. These photographs demonstrate this novel material is space-saving, light-weight, and easy to cut and manipulate into different shapes. The paper-based electrode with sputtered Pt is shown in Fig. 3b for comparison. Fig. 3d–e present top-view and side-view (inset) SEM images of the paper-based electrodes made with 30 vol% GD/PEDOT:PSS and sputtered Pt, respectively. The corresponding images at higher magnification are shown in Fig. S6. These images reveal that the porosity of the paper substrate can be effectively filled with the GD/PEDOT:PSS composite, while the porous features still remain visible even after sputtering the sample with Pt. The results indicate that the sputtered Pt layer is not likely to facilitate efficient electron transport within the porous matrix of the paper substrate.

We then integrated the two paper-based counter electrodes with the flexible dye/TiO2/ITO-PEN photoanodes (Fig. 3c) to fabricate the flexible DSSCs. Fig. 3f shows the J-V curves of the flexible DSSCs made using the 30 vol% GD/PEDOT:PSS and sputtered Pt paper counter

electrodes. The corresponding photovoltaic parameters are listed in Table 3. The flexible DSSC made with the GD/PEDOT:PSS paper counter electrode exhibited an η (4.91%) that was almost three times higher than that of the cell made with the sputtered Pt paper counter electrode (1.70%). We attributed this difference to the im-proved charge transport in the less porous GD/PEDOT:PSS paper electrode. This is the opposite result we observed for the FTO-based counter electrodes (Table 1), in which the non-porous FTO glass substrate provided a continuous conducting layer. Although the η of the device is lower when the paper-based substrate is used, replacing the FTO-based counter electrode with a metal-free substitute can significantly reduce the manufacturing costs of the DSSC.

In addition, the GD/PEDOT:PSS paper-based counter electrode provides the DSSC with flexibility in a way that cannot be achieved when FTO is used as substrate instead. As a comparison of the sputtered Pt and GD/PEDOT:PSS paper electrodes, Fig. 3g presents the normalized η of the two flexible DSSCs after bending the electrodes up to 150 times. The non-normalized photovoltaic parameters (i.e., η, FF, VOC, JSC) of the two devices are shown in Fig. S7. From these results, we can see that η of the flexible DSSC made using the GD/PEDOT:PSS paper electrode remained fairly stable even after being bent 150 times, while η of the flexible DSSC made using the sputtered Pt paper electrode decreased by 45% after the same test. This result demonstrates the amazing durability of the paper-based GD/PEDOT:PSS counter electrode to a degree that cannot be achieved by its Pt counterpart.

4. Conclusions

We synthesized a GD/PEDOT:PSS composite ink for the fabrication of Pt-free counter electrodes for use in DSSCs. On FTO-based counter electrodes, the DSSC device made using 30 vol% GD/PEDOT:PSS exhibited an optimal cell efficiency of 7.36%, which was comparable with that made with sputtered Pt (8.46%). We also fabricated a flexible paper-

based counter electrode made with the same 30 vol% GD/PEDOT:PSS composite using a cost-effective “soak and dry” method that can be easily scaled up for mass production. Flexible DSSCs made on paper-based counter electrodes featuring this GD/PEDOT:PSS ink exhibited cell efficiencies (4.91%) that were much higher than that of sputtered Pt paper electrodes (1.70%) due to the fact that the polymer and GDs-based ink was better able to fill the pores of the paper substrate, while sputter coating was unable to sufficiently reach all the surfaces and coat the metal inside all the voids. After bending the paper electrodes 150 times, we found that the performance of the cell with the GD/PEDOT:PSS paper electrode was well preserved, while in contrast the device made using sputtered Pt drastically lost its initial cell performance after the same test. The presented GD/PEDOT:PSS paper electrode is low-cost, light-weight, space-saving, environmentally friendly, and easy to manipulate, all of which demonstrate the potential of this composite material for portable/wearable electronics and flexible energy systems.

Acknowledgements

This work was financially supported by the King Abdullah University of Science and Technology (KAUST) Office of Sponsored Research (OSR)(OSR-2016-CRG5-3005), KAUST solar center (FCC/1/3079-08-01), KAUST baseline funding, the Research Grants Council of Hong Kong (PolyU 153012/14P), the National Natural Science Foundation of China (11374250), and National Taiwan University (102R4000).

References

[1] D. Tobjörk, R. Österbacka, Paper electronics, Adv. Mater. 23 (2011) 1935–1961.

[2] C. Wang, D. Hwang, Z. Yu, K. Takei, J. Park, T. Chen, B. Ma, A. Javey, Userinteractive electronic skin for instantaneous pressure visualization, Nat. Mater. 12

(2013) 899–904.

[3] H. Zhu, Z. Xiao, D. Liu, Y. Li, N.J. Weadock, Z. Fang, J. Huang, L. Hu, Biodegradable transparent substrates for flexible organic-light-emitting diodes, Energy Environ. Sci. 6 (2013) 2105–2111.

[4] M. Härting, J. Zhang, D.R. Gamota, D.T. Britton, Fully printed silicon field effect transistors, Appl. Phys. Lett. 94 (2009) 193509.

[5] P. Andersson, D. Nilsson, P.O. Svensson, M. Chen, A. Malmström, T. Remonen, T. Kugler, M. Berggren, Active matrix displays based on all-organic electrochemical smart pixels printed on paper, Adv. Mater. 14 (2002) 1460–1464.

[6] V. Lakafosis, A. Rida, R. Vyas, L. Yang, S. Nikolaou, M.M. Tentzeris, Progress towards the first wireless sensor networks consisting of inkjet-printed, paper-based RFID-enabled sensor tags, Proc. IEEE 98 (2010) 1601–1609.

[7] D.-H. Lien, Z.-K. Kao, T.-H. Huang, Y.-C. Liao, S.-C. Lee, J.-H. He, All-printed paper memory, ACS Nano 8 (2014) 7613–7619.

[8] L. Hu, H. Wu, F. La Mantia, Y. Yang, Y. Cui, Thin, flexible secondary Li-ion paper batteries, ACS Nano 4 (2010) 5843–5848.

[9] X. Chen, H. Zhu, C. Liu, Y.-C. Chen, N. Weadock, G. Rubloff, L. Hu, Role of mesoporosity in cellulose fibers for paper-based fast electrochemical energy storage, J. Mater. Chem. A 1 (2013) 8201–8208.

[10] L. Yuan, X. Xiao, T. Ding, J. Zhong, X. Zhang, Y. Shen, B. Hu, Y. Huang, J. Zhou, Z.L. Wang, Paper-based supercapacitors for self-powered nanosystems, Angew. Chem. Int. Ed. 51 (2012) 4934–4938.

[11] G. Zheng, L. Hu, H. Wu, X. Xie, Y. Cui, Paper supercapacitors by a solvent-free drawing method, Energy Environ. Sci. 4 (2011) 3368–3373.

[12] Z. Gui, H. Zhu, E. Gillette, X. Han, G.W. Rubloff, L. Hu, S.B. Lee, Natural cellulose

fiber as substrate for supercapacitor, ACS Nano 7 (2013) 6037–6046.

[13] L. Hu, G. Zheng, J. Yao, N. Liu, B. Weil, M. Eskilsson, E. Karabulut, Z. Ruan, S. Fan, J.T. Bloking, M.D. McGehee, L. Wagberg, Y. Cui, Transparent and conductive paper from nanocellulose fibers, Energy Environ. Sci. 6 (2013) 513–518.

[14] Z. Fang, H. Zhu, Y. Yuan, D. Ha, S. Zhu, C. Preston, Q. Chen, Y. Li, X. Han, S. Lee, G. Chen, T. Li, J. Munday, J. Huang, L. Hu, Novel nanostructured paper with ultrahigh transparency and ultrahigh haze for solar cells, Nano Lett. 14 (2014) 765–773.

[15] A.R. Yugis, R.F. Mansa, C.S. Sipaut, Review on metallic and plastic flexible dye sensitized solar cell, IOP Conf. Ser.: Mater. Sci. Eng. 78 (2015) 012003.

[16] K. Fan, T. Peng, J. Chen, X. Zhang, R. Li, Low-cost, quasi-solid-state and TCO-free highly bendable dye-sensitized cells on paper substrate, J. Mater. Chem. 22 (2012) 16121–16126.

[17] B. O'Regan, M. Gratzel, A low-cost, high-efficiency solar cell based on dyesensitized colloidal TiO2 films, Nature 353 (1991) 737–740.

[18] K. Yoo, J.-Y. Kim, J.A. Lee, J.S. Kim, D.-K. Lee, K. Kim, J.Y. Kim, B. Kim, H. Kim, W.M. Kim, J.H. Kim, M.J. Ko, Completely transparent conducting oxide-free and flexible dye-sensitized solar cells fabricated on plastic substrates, ACS Nano 9 (2015) 3760–3771.

[19] S. Ahmad, E. Dell'Orto, J.-H. Yum, F. Kessler, M.K. Nazeeruddin, M. Gratzel, Towards flexibility: metal free plastic cathodes for dye sensitized solar cells, Chem. Commun. 48 (2012) 9714–9716.

[20] J. Idigoras, E. Guillen, F.J. Ramos, J.A. Anta, M.K. Nazeeruddin, S. Ahmad, Highly efficient flexible cathodes for dye sensitized solar cells to complement Pt@TCO coatings, J. Mater. Chem. A 2 (2014) 3175–3181.

[21] I.T. Chiu, C.-T. Li, C.-P. Lee, P.-Y. Chen, Y.-H. Tseng, R. Vittal, K.-C. Ho, Nanoclimbing-wall-like CoSe2/carbon composite film for the counter electrode of a highly efficient dye-sensitized solar cell: a study on the morphology control, Nano Energy 22 (2016) 594–606.

[22] M. Wu, T. Ma, Platinum-free catalysts as counter electrodes in dye-sensitized solar cells, ChemSusChem 5 (2012) 1343–1357.

[23] C.-P. Lee, C.-A. Lin, T.-C. Wei, M.-L. Tsai, Y. Meng, C.-T. Li, K.-C. Ho, C.-I Wu, S.-P. Lau, J.-H. He, Economical low-light photovoltaics by using the Pt-free dyesensitized solar cell with graphene dot/PEDOT:PSS counter electrodes, Nano Energy 18 (2015) 109–117.

[24] H. Wang, Y.H. Hu, Graphene as a counter electrode material for dye-sensitized solar cells, Energy Environ. Sci. 5 (2012) 8182–8188.

[25] Y. Xue, J. Liu, H. Chen, R. Wang, D. Li, J. Qu, L. Dai, Nitrogen-doped graphene foams as metal-free counter electrodes in high-performance dye-sensitized solar cells, Angew. Chem. Int. Ed. 51 (2012) 12124–12127.

[26] C.-T. Li, C.-P. Lee, M.-S. Fan, P.-Y. Chen, R. Vittal, K.-C. Ho, Ionic liquid-doped poly(3,4-ethylenedioxythiophene) counter electrodes for dye-sensitized solar cells: cationic and anionic effects on the photovoltaic performance, Nano Energy 9 (2014) 1–14.

[27] L.-Y. Chang, C.-T. Li, Y.-Y. Li, C.-P. Lee, M.-H. Yeh, K.-C. Ho, J.-J. Lin, Morphological Influence of polypyrrole nanoparticles on the performance of dye–sensitized solar cells, Electrochim. Acta 155 (2015) 263–271.

[28] M.S. Rahman, W.A. Hammed, R.B. Yahya, H. Mahmud, Prospects of conducting polymer and graphene as counter electrodes in dye-sensitized solar cells, J. Polym. Res. 23 (2016).

[29] H. Shirakawa, E.J. Louis, A.G. MacDiarmid, C.K. Chiang, A.J. Heeger, Synthesis of electrically conducting organic polymers: halogen derivatives of polyacetylene, (CH)x, J. Chem. Soc. Chem. Commun. (1977) 578–580.

[30] C.K. Chiang, M.A. Druy, S.C. Gau, A.J. Heeger, E.J. Louis, A.G. MacDiarmid, Y.W. Park, H. Shirakawa, Synthesis of highly conducting films of derivatives of polyacetylene, (CH)x, J. Am. Chem. Soc. 100 (1978) 1013–1015.

[31] V.K. Thakur, G. Ding, J. Ma, P.S. Lee, X. Lu, Hybrid materials and polymer electrolytes for electrochromic device applications, Adv. Mater. 24 (2012) 4071–4096.

[32] J. Ha, S. Chung, M. Pei, K. Cho, H. Yang, Y. Hong, One-step interface engineering for all-inkjet-printed, all-organic components in transparent, flexible transistors and inverters: polymer binding, ACS Appl. Mater. Interfaces 9 (2017) 8819–8829.

[33] B. Sanyoto, S. Kim, W.T. Park, Y. Xu, J.H. Kim, J.C. Lim, Y.Y. Noh, Solution processable PEDOT:PSS based hybrid electrodes for organic field effect transistors, Org. Electron.: Phys. Mater. Appl. 37 (2016) 352–357.

[34] F. Wang, L. Zhu, J. Zhang, Electrochemical sensor for levofloxacin based on molecularly imprinted polypyrrole-graphene-gold nanoparticles modified electrode, Sens. Actuators B: Chem. 192 (2014) 642–647.

[35] L. Al-Mashat, K. Shin, K. Kalantar-Zadeh, J.D. Plessis, S.H. Han, R.W. Kojima, R.B. Kaner, D. Li, X. Gou, S.J. Ippolito, W. Wlodarski, Graphene/polyaniline nanocomposite for hydrogen sensing, J. Phys. Chem. C 114 (2010) 16168–16173.

[36] A. Burke, Ultracapacitors: why, how, and where is the technology, J. Power Sources 91 (2000) 37–50.

[37] L.M. Santino, Y. Lu, S. Acharya, L. Bloom, D. Cotton, A. Wayne, J.M. D'Arcy, Enhancing cycling stability of aqueous polyaniline electrochemical capacitors, ACS

Appl. Mater. Interfaces 8 (2016) 29452–29460.

[38] C.J. Zhang, T.M. Higgins, S.H. Park, S.E. O'Brien, D. Long, J.N. Coleman, V. Nicolosi, Highly flexible and transparent solid-state supercapacitors based on RuO2/PEDOT:PSS conductive ultrathin films, Nano Energy 28 (2016) 495–505.

[39] A.A. Argun, A. Cirpan, J.R. Reynolds, The first truly all-polymer electrochromic devices, Adv. Mater. 15 (2003) 1338–1341.

[40] H.J. Shin, S.S. Jeon, S.S. Im, CNT/PEDOT core/shell nanostructures as a counter electrode for dye-sensitized solar cells, Synth. Met. 161 (2011) 1284–1288.

[41] C.-H. Chiang, C.-G. Wu, High-efficient dye-sensitized solar cell based on highly conducting and thermally stable PEDOT:PSS/glass counter electrode, Org. Electron. 14 (2013) 1769–1776.

[42] T.H. Lee, K. Do, Y.W. Lee, S.S. Jeon, C. Kim, J. Ko, S.S. Im, High-performance dyesensitized
solar cells based on PEDOT nanofibers as an efficient catalytic counter electrode, J. Mater. Chem. 22 (2012) 21624.

[43] C.T. Li, C.P. Lee, M.S. Fan, P.Y. Chen, R. Vittal, K.C. Ho, Ionic liquid-doped poly(3,4-ethylenedioxythiophene) counter electrodes for dye-sensitized solar cells: cationic and anionic effects on the photovoltaic performance, Nano Energy 9 (2014) 1–14.

[44] P.Y. Chen, C.T. Li, C.P. Lee, R. Vittal, K.C. Ho, PEDOT-decorated nitrogen-doped graphene as the transparent composite film for the counter electrode of a dyesensitized solar cell, Nano Energy 12 (2015) 374–385.

[45] J. Zhang, N. Vlachopoulos, M. Jouini, M.B. Johansson, X. Zhang, M.K. Nazeeruddin, G. Boschloo, E.M.J. Johansson, A. Hagfeldt, Efficient solid-state dye sensitized solar cells: the influence of dye molecular structures for the in-situ

photoelectrochemically polymerized PEDOT as hole transporting material, Nano Energy 19 (2016) 455–470.

[46] K. Manseki, W. Jarernboon, Y. Youhai, K.-J. Jiang, K. Suzuki, N. Masaki, Y. Kim, J. Xia, S. Yanagida, Solid-state dye-sensitized solar cells fabricated by coupling photoelectrochemically deposited poly(3,4-ethylenedioxythiophene) (PEDOT) with silver-paint on cathode, Chem. Commun. 47 (2011) 3120–3122.

[47] Y. Xu, Y. Wang, J. Liang, Y. Huang, Y. Ma, X. Wan, Y. Chen, A hybrid material of graphene and poly (3,4-ethyldioxythiophene) with high conductivity, flexibility, and transparency, Nano Res. 2 (2009) 343–348.

[48] J.-G. Chen, H.-Y. Wei, K.-C. Ho, Using modified poly(3,4-ethylene dioxythiophene): poly(styrene sulfonate) film as a counter electrode in dye-sensitized solar cells, Sol. Energy Mater. Sol. Cells 91 (2007) 1472–1477.

[49] K. Koji, S. Seimei, Layer-by-layer self-assembled mesoporous PEDOT–PSS and carbon black hybrid films for platinum free dye-sensitized-solar-cell counter electrodes, Nanotechnology 22 (2011) 195703.

[50] G. Yue, J. Wu, Y. Xiao, J. Lin, M. Huang, Low cost poly(3,4-ethylenedioxythiophene): polystyrenesulfonate/carbon black counter electrode for dye-sensitized solar cells, Electrochim. Acta 67 (2012) 113–118.

[51] W. Hong, Y. Xu, G. Lu, C. Li, G. Shi, Transparent graphene/PEDOT–PSS composite films as counter electrodes of dye-sensitized solar cells, Electrochem. Commun. 10 (2008) 1555–1558.

[52] J. Shen, Y. Zhu, X. Yang, C. Li, Graphene quantum dots: emergent nanolights for bioimaging, sensors, catalysis and photovoltaic devices, Chem. Commun. 48 (2012) 3686–3699.

[53] T.-F. Yeh, C.-Y. Teng, S.-J. Chen, H. Teng, Nitrogen-doped graphene oxide

quantum dots as photocatalysts for overall water-splitting under visible light illumination, Adv. Mater. 26 (2014) 3297–3303.

[54] H. Sun, L. Wu, N. Gao, J. Ren, X. Qu, Improvement of photoluminescence of graphene quantum dots with a biocompatible photochemical reduction pathway and its bioimaging application, ACS Appl. Mater. Interfaces 5 (2013) 1174–1179.

[55] S. Zhu, J. Zhang, C. Qiao, S. Tang, Y. Li, W. Yuan, B. Li, L. Tian, F. Liu, R. Hu, H. Gao, H. Wei, H. Zhang, H. Sun, B. Yang, Strongly green-photoluminescent graphene quantum dots for bioimaging applications, Chem. Commun. 47 (2011) 6858–6860.

[56] D.I. Son, B.W. Kwon, D.H. Park, W.-S. Seo, Y. Yi, B. Angadi, C.-L. Lee, W.K. Choi, Emissive ZnO-graphene quantum dots for white-light-emitting diodes, Nat. Nano 7 (2012) 465–471.

[57] L. Tang, R. Ji, X. Cao, J. Lin, H. Jiang, X. Li, K.S. Teng, C.M. Luk, S. Zeng, J. Hao, S.P. Lau, Deep ultraviolet photoluminescence of water-soluble self-passivated graphene quantum dots, ACS Nano 6 (2012) 5102–5110.

[58] M.-L. Tsai, W.-R. Wei, L. Tang, H.-C. Chang, S.-H. Tai, P.-K. Yang, S.P. Lau, L.-J. Chen, J.-H. He, Si hybrid solar cells with 13% efficiency via concurrent improvement in optical and electrical properties by employing graphene quantum dots, ACS Nano 10 (2016) 815–821.

[59] V. Gupta, N. Chaudhary, R. Srivastava, G.D. Sharma, R. Bhardwaj, S. Chand, Luminescent graphene quantum dots for organic photovoltaic devices, J. Am. Chem. Soc. 133 (2011) 9960–9963.

[60] L. Chen, C.X. Guo, Q. Zhang, Y. Lei, J. Xie, S. Ee, G. Guai, Q. Song, C.M. Li, Graphene quantum-dot-doped polypyrrole counter electrode for high-performance dye-sensitized solar cells, ACS Appl. Mater. Interfaces 5 (2013) 2047–2052.

[61] E. Lee, J. Ryu, J. Jang, Fabrication of graphene quantum dots via size-selective precipitation and their application in upconversion-based DSSCs, Chem. Commun. 49 (2013) 9995–9997.

[62] C.-A. Lin, C.-P. Lee, S.-T. Ho, T.-C. Wei, Y.-W. Chi, K.P. Huang, J.-H. He, Nitrogendoped graphene/platinum counter electrodes for dye-sensitized solar cells, ACS Photonics 1 (2014) 1264–1269.

[63] C.-P. Lee, L.-Y. Lin, K.-W. Tsai, R. Vittal, K.-C. Ho, Enhanced performance of dyesensitized solar cell with thermally-treated TiN in its TiO2 film prepared at low temperature, J. Power Sources 196 (2011) 1632–1638.

[64] L.-Y. Lin, P.-C. Nien, C.-P. Lee, K.-W. Tsai, M.-H. Yeh, R. Vittal, K.-C. Ho, Lowtemperature flexible photoanode and net-like Pt counter electrode for improving the performance of dye-sensitized solar cells, J. Phys. Chem. C 114 (2010) 21808–21815.

[65] L.-Y. Lin, C.-P. Lee, K.-W. Tsai, M.-H. Yeh, C.-Y. Chen, R. Vittal, C.-G. Wu, K.-C. Ho, Low-temperature flexible Ti/TiO2 photoanode for dye-sensitized solar cells with binder-free TiO2 paste, Prog. Photovolt.: Res. Appl. 20 (2012) 181–190.

[66] Y. Dong, J. Lin, Y. Chen, F. Fu, Y. Chi, G. Chen, Graphene quantum dots, graphene oxide, carbon quantum dots and graphite nanocrystals in coals, Nanoscale 6 (2014) 7410–7415.

[67] A.C. Ferrari, Raman spectroscopy of graphene and graphite: disorder, electron–phonon coupling, doping and nonadiabatic effects, Solid State Commun. 143 (2007) 47–57.

[68] Z. Luo, T. Yu, K.-J. Kim, Z. Ni, Y. You, S. Lim, Z. Shen, S. Wang, J. Lin, Thicknessdependent
reversible hydrogenation of graphene layers, ACS Nano 3 (2009)
1781–1788.
[69] C. Punckt, M.A. Pope, J. Liu, Y. Lin, I.A. Aksay, Electrochemical performance of graphene as effected by electrode porosity and graphene functionalization, Electroanalysis 22 (2010) 2834–2841.
[70] G. Yue, J. Wu, Y. Xiao, J. Lin, M. Huang, Z. Lan, L. Fan, Functionalized graphene/ poly(3,4-ethylenedioxythiophene):polystyrenesulfonate as counter electrode catalyst for dye-sensitized solar cells, Energy 54 (2013) 315–321.
[71] M.-H. Yeh, L.-Y. Lin, C.-P. Lee, H.-Y. Wei, C.-Y. Chen, C.-G. Wu, R. Vittal, K.-C. Ho, A composite catalytic film of PEDOT:PSS/TiN-NPs on a flexible counter-electrode substrate for a dye-sensitized solar cell, J. Mater. Chem. 21 (2011) 19021–19029.

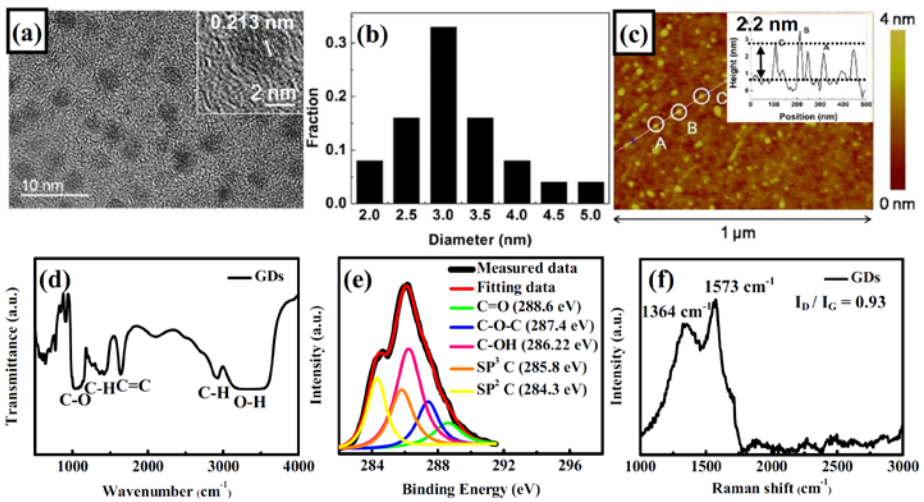

Fig. 1. (a) TEM image of the GDs and a corresponding high resolution image (inset). (b) The diameter distribution of the GDs from the sample shown in (a), measured via TEM. (c) AFM image of the GDs and the corresponding height profile across three individual GDs. (d) FTIR, (e) XPS, and (f) Raman spectra of the GDs sample.

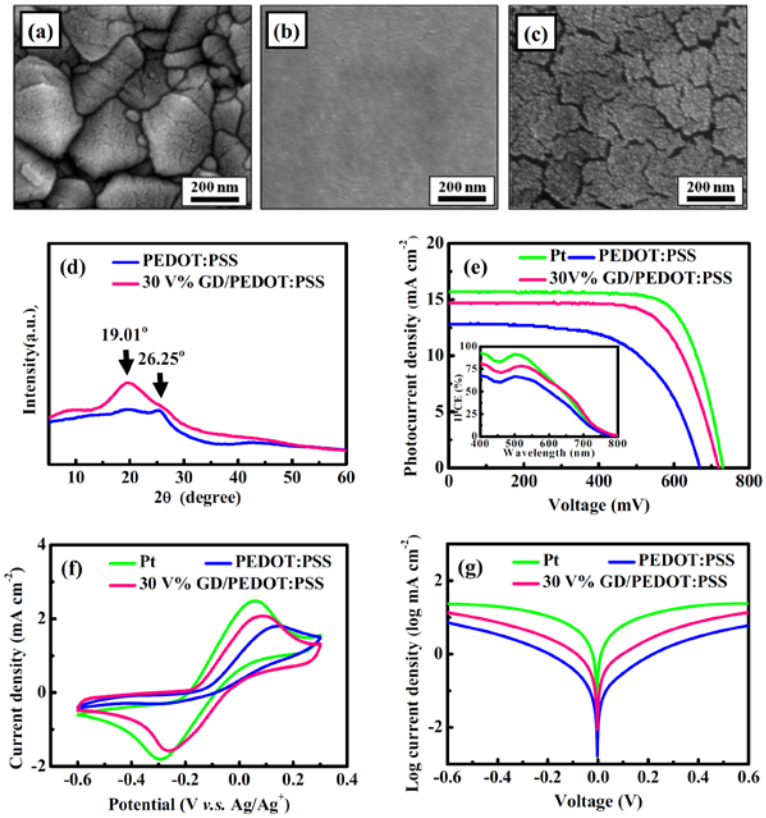

Fig. 2. SEM images of the counter electrodes featuring (a) sputtered Pt, (b) PEDOT:PSS, and (c) 30 vol% GD/PEDOT:PSS on FTO substrates. (d) XRD patterns of the PEDOT:PSS film with and without the addition of GDs. (e) The *J-V* curves of DSSCs made with the three types of counter electrodes on FTO substrates. Their corresponding IPCE curves are shown in the inset. (f) CV of the three counter electrodes using FTO substrates, which was carried out in a three-electrode system. (g) The Tafel polarization curves of the three types of counter electrodes using FTO substrates.

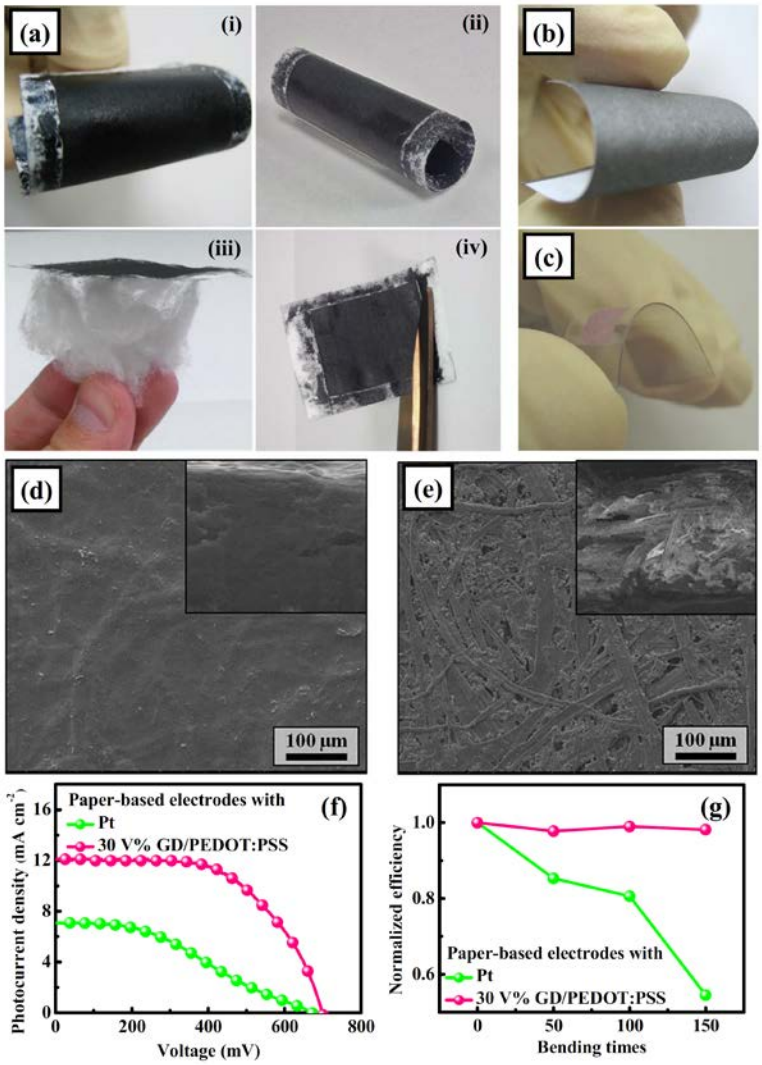

Fig. 3. (a) Images of the paper-based counter electrodes made with the 30 vol% GD/PEDOT:PSS composite demonstrate the material is (i) flexible, (ii) space-saving, (iii) light-weight, and (iv) easy to cut. (b) Image of the paper-based counter electrode made with sputtered Pt. (c) A flexible dye-sensitized TiO_2 photoanode using the ITO-PEN substrate. (d) Top-view and side-view (inset) SEM images of the paper-based counter electrode made with the 30 vol% GD/PEDOT:PSS composite. (e) Top-view and side-view (inset) SEM images of the paper-based counter electrode made with sputtered Pt. (f) The *J-V* curves of the flexible DSSCs using the two types of paper-based counter electrodes. (g) Normalized efficiency of the flexible DSSCs using the two types of paper-based counter electrodes after being bent up to 150 times. Both of the flexible DSSCs used the dye/TiO_2/ITO-PEN photoanode substrate.